Effect of Polymer Architecture on Phase Behavior and Structure of Polyelectrolyte/Microemulsion Complexes (PEMECs)

Supporting Material

Miriam Simon[1]*, Emanuel Schneck[2], Laurence Noirez[3], Sofia Rahn[1], Irina Davidovich[4], Yeshayahu Talmon[4], and Michael Gradzielski[1]*

1: Stranski-Laboratorium für Physikalische und Theoretische Chemie, Institut für Chemie, Technische Universität Berlin, 10623 Berlin, Germany
2: Physics Department, Technische Universität Darmstadt, 64289 Darmstadt, Germany
3: Laboratoire Léon Brillouin (CEA-CNRS), Uni. Paris-Saclay, CEA-Saclay, 91191 Gif-sur-Yvette, France
4: Department of Chemical Engineering and the Russell Berrie Nanotechnology Institute (RBNI), Technion – Israel Institute of Technology, Haifa, 3200003, Israel

miriam.simon@tu-berlin.de
michael.gradzielski@tu-berlin.de

Contents

A. Sample Compositions

Table S1: Exact compositions of all studied samples.

	TDMAO / mM	TTAB / mM	Hexanol / mM	Decane / mM	PE / wt%
ME00-00	94.45	5.01	0.00	30.37	0.00
ME00-NaHA51-0.05	93.72	4.97	0.00	30.14	0.01
ME00-NaHA51-0.1	94.71	5.02	0.00	30.46	0.02
ME00-NaHA51-0.2	94.57	5.02	0.00	30.42	0.04
ME00-NaHA51-0.3	94.32	5.00	0.00	30.33	0.08
ME00-NaHA51-0.4	94.29	5.00	0.00	30.32	0.12
ME00-NaHA51-0.5	94.47	5.01	0.00	30.38	0.18
ME00-NaHA51-0.6	93.87	4.98	0.00	30.19	0.27
ME00-NaHA51-0.65	94.78	5.03	0.00	30.48	0.32
ME00-NaHA51-0.7	94.16	4.99	0.00	30.28	0.42
ME00-NaHA51-0.8	94.41	5.01	0.00	30.36	0.72
ME00-NaHA51-0.9	93.41	4.95	0.00	30.04	1.57
ME00-NaHA150-0.05	93.77	4.97	0.00	30.16	0.01
ME00-NaHA150-0.6	93.26	4.95	0.00	30.00	0.28
ME00-NaHA150-0.7	93.81	4.97	0.00	30.17	0.43
ME00-NaHA150-0.8	94.22	5.00	0.00	30.30	0.72
ME00-NaHA150-0.9	94.12	4.99	0.00	30.27	1.56
ME00-NaHA360-0.05	93.05	4.94	0.00	29.93	0.01
ME00-NaHA360-0.6	94.07	4.99	0.00	30.25	0.27
ME00-NaHA360-0.7	94.23	5.00	0.00	30.31	0.41
ME00-NaHA360-0.8	95.02	5.04	0.00	30.56	0.70
ME00-NaHA360-0.9	93.88	4.98	0.00	30.19	1.57
ME00-NaHA800-0.05	94.05	4.99	0.00	30.25	0.01
ME00-NaHA800-0.6	93.76	4.97	0.00	30.15	0.27
ME00-NaHA800-0.7	93.52	4.96	0.00	30.08	0.41
ME00-NaHA800-0.8	93.82	4.98	0.00	30.18	0.72
ME00-NaHA800-0.9	93.78	4.97	0.00	30.16	1.56
ME50-00	93.53	4.91	49.87	80.58	0.00
ME50-NaHA51-0.05	94.18	4.94	50.23	81.15	0.01
ME50-NaHA51-0.1	93.55	4.91	49.89	80.61	0.02
ME50-NaHA51-0.2	94.41	4.96	50.35	81.35	0.04
ME50-NaHA51-0.3	94.52	4.96	50.41	81.44	0.07
ME50-NaHA51-0.4	94.66	4.97	50.48	81.56	0.11
ME50-NaHA51-0.5	94.41	4.96	50.35	81.35	0.18
ME50-NaHA51-0.6	93.42	4.90	49.82	80.49	0.26
ME50-NaHA51-0.65	94.16	4.94	50.21	81.13	0.32
ME50-NaHA51-0.7	91.74	4.81	48.92	79.04	0.39
ME50-NaHA51-0.8	86.01	4.51	45.87	74.11	0.63
ME50-NaHA51-0.9	94.84	4.98	50.57	81.71	1.55
ME50-NaHA150-0.05	93.87	4.93	50.06	80.88	0.01
ME50-NaHA150-0.1	93.14	4.89	49.67	80.25	0.02
ME50-NaHA150-0.65	93.96	4.93	50.11	80.96	0.32
ME50-NaHA150-0.7	94.14	4.94	50.20	81.11	0.40
ME50-NaHA150-0.8	94.37	4.95	50.33	81.31	0.69
ME50-NaHA150-0.9	94.39	4.95	50.33	81.33	1.55

	TDMAO / mM	TTAB / mM	Hexanol / mM	Decane / mM	PE / wt%
ME50-NaHA360-0.05	94.03	4.94	50.14	81.02	0.01
ME50-NaHA360-0.1	93.81	4.92	50.03	80.83	0.02
ME50-NaHA360-0.65	91.79	4.82	48.95	79.09	0.31
ME50-NaHA360-0.7	94.39	4.95	50.33	81.33	0.41
ME50-NaHA360-0.8	93.68	4.92	49.96	80.72	0.70
ME50-NaHA360-0.9	93.44	4.90	49.83	80.51	1.58
ME50-NaHA800-0.05	93.41	4.90	49.81	80.48	0.01
ME50-NaHA800-0.1	94.10	4.94	50.18	81.08	0.02
ME50-NaHA800-0.65	94.10	4.94	50.18	81.08	0.33
ME50-NaHA800-0.7	94.50	4.96	50.39	81.42	0.40
ME50-NaHA800-0.8	93.85	4.93	50.05	80.86	0.70
ME50-NaHA800-0.9	89.38	4.69	47.66	77.01	1.50
ME75-00	94.71	5.06	75.70	198.40	0.00
ME75-NaHA51-0.05	94.65	5.05	75.65	198.27	0.01
ME75-NaHA51-0.1	95.96	5.12	76.69	201.01	0.02
ME75-NaHA51-0.6	94.29	5.03	75.36	197.52	0.27
ME75-NaHA51-0.65	98.48	5.26	78.71	206.30	0.33
ME75-NaHA51-0.7	92.98	4.96	74.31	194.77	0.38
ME75-NaHA51-0.8	94.71	5.06	75.70	198.40	0.68
ME75-NaHA51-0.9	95.42	5.09	76.26	199.88	1.53
ME75-NaHA150-0.7	95.12	5.08	76.03	199.26	0.41
ME75-NaHA150-0.8	94.68	5.05	75.67	198.33	0.69
ME75-NaHA150-0.9	95.40	5.09	76.25	199.84	1.53
ME75-NaHA360-0.7	95.09	5.08	76.00	199.19	0.39
ME75-NaHA360-0.8	94.51	5.05	75.53	197.97	0.68
ME75-NaHA360-0.9	94.13	5.03	75.23	197.19	1.54
ME75-NaHA800-0.7	94.96	5.07	75.89	198.92	0.41
ME75-NaHA800-0.8	94.99	5.07	75.92	198.98	0.68
ME75-NaHA800-0.9	95.04	5.07	75.96	199.08	1.53
ME00-NaCMC90-0.7	93.99	4.98	0.00	30.23	0.31
ME00-NaCMC90-0.8	94.07	4.99	0.00	30.25	0.57
ME00-NaCMC90-0.9	93.88	4.98	0.00	30.19	1.24
ME00-NaCMC250-0.6	94.00	4.99	0.00	30.23	0.25
ME00-NaCMC250-0.7	94.90	5.03	0.00	30.52	0.38
ME00-NaCMC250-0.8	93.96	4.98	0.00	30.22	0.65
ME00-NaCMC250-0.9	94.19	5.00	0.00	30.29	1.47
ME50-NaCMC90-0.05	94.92	4.97	50.15	81.23	0.01
ME50-NaCMC90-0.1	95.09	4.98	50.23	81.37	0.02
ME50-NaCMC90-0.6	95.61	5.01	50.51	81.81	0.20
ME50-NaCMC90-0.7	95.33	4.99	50.36	81.58	0.32
ME50-NaCMC90-0.8	95.28	4.99	50.34	81.54	0.54
ME50-NaCMC90-0.9	95.08	4.98	50.23	81.36	1.22
ME50-NaCMC250-0.05	95.08	4.98	50.23	81.36	0.01
ME50-NaCMC250-0.1	95.23	4.99	50.31	81.50	0.02
ME50-NaCMC250-0.6	95.28	4.99	50.34	81.54	0.24
ME50-NaCMC250-0.7	94.85	4.97	50.11	81.17	0.38
ME50-NaCMC250-0.8	96.61	5.06	51.04	82.68	0.64
ME50-NaCMC250-0.9	96.64	5.06	51.06	82.70	1.45

	TDMAO / mM	TTAB / mM	Hexanol / mM	Decane / mM	PE / wt%
ME75-NaCMC90-0.7	94.79	5.06	75.76	198.56	0.31
ME75-NaCMC90-0.8	94.79	5.06	75.76	198.56	0.53
ME75-NaCMC90-0.9	94.79	5.06	75.76	198.56	1.19
ME75-NaCMC250-0.7	94.79	5.06	75.76	198.56	0.21
ME75-NaCMC250-0.8	94.79	5.06	75.76	198.56	0.37
ME75-NaCMC250-0.9	94.79	5.06	75.76	198.56	0.82

B. Phase Behavior
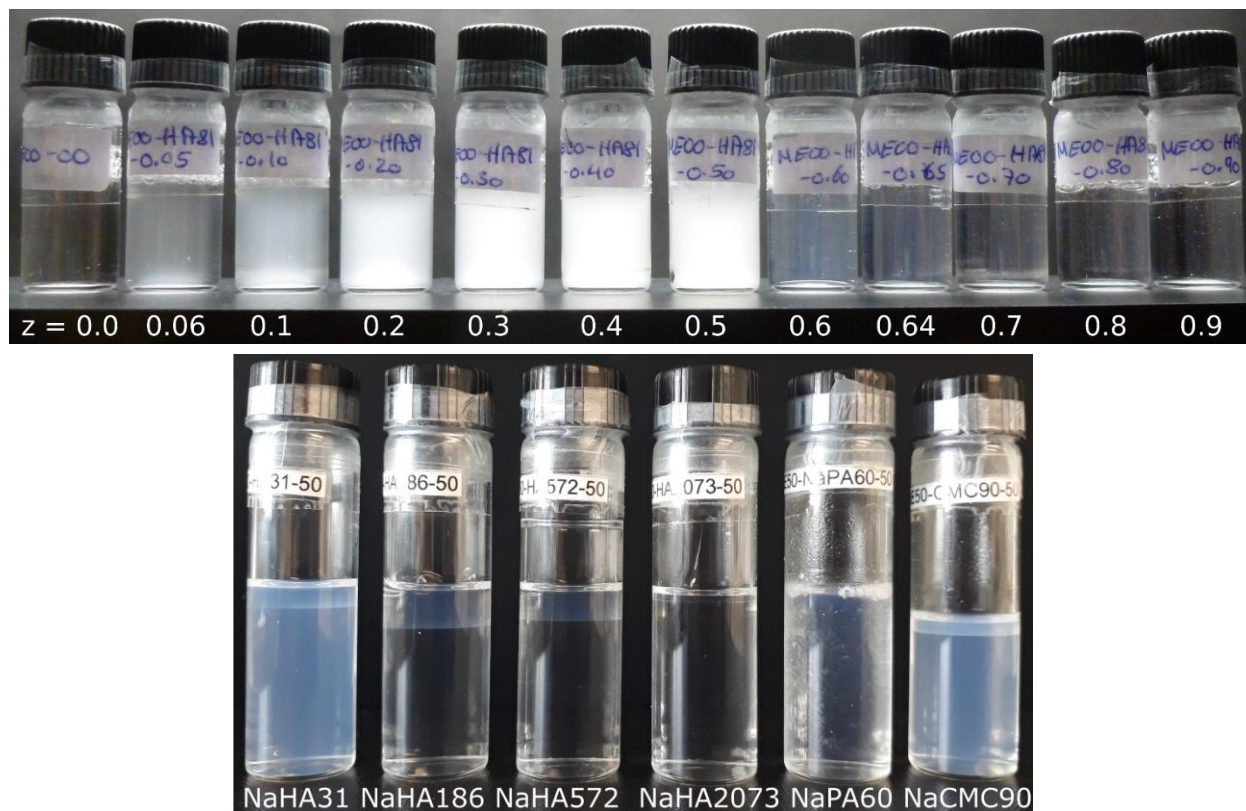
Figure S1: Top: photograph of samples of ME00 (R = 3.1 nm) and NaHA (M_w =51 kDa), 1 week old, shaken before taking the photo. Bottom: photograph showing the phase separation into two liquid phases of samples of ME50 (R = 4.1 nm) and different polyelectrolytes at z = 0.5 (taken after a resting for one day).
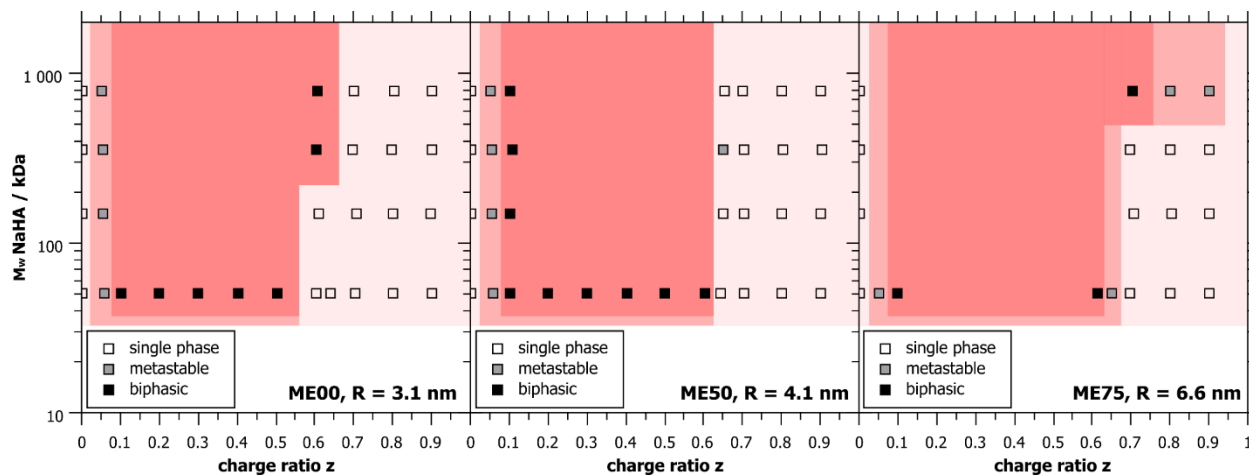
Figure S2: Phase diagrams showing the single phase, metastable and biphasic regions of differently sized microemulsion droplets mixed with NaHA.
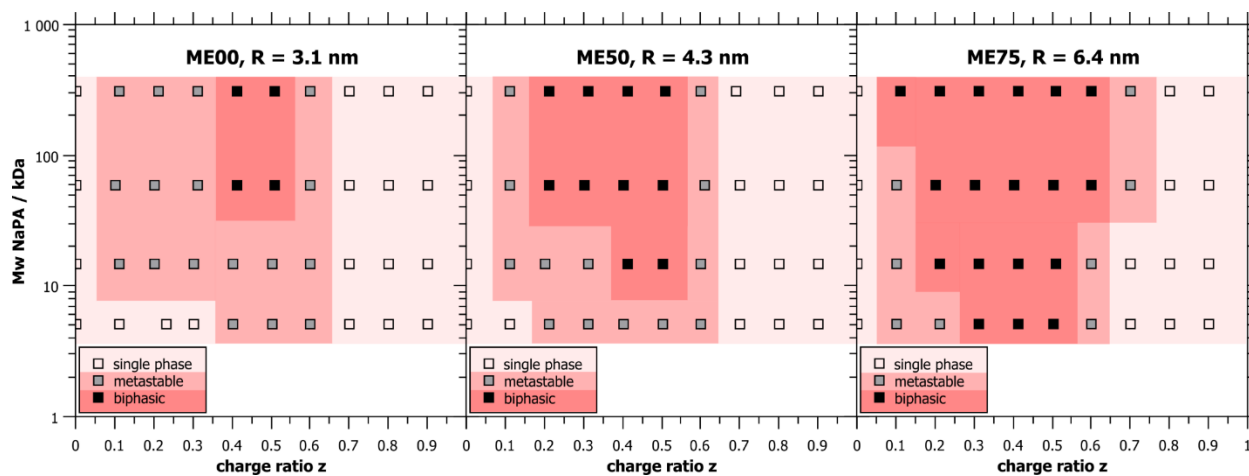
Figure S3: Phase diagrams showing the single phase, metastable and biphasic regions of differently sized microemulsion droplets mixed with NaPA. Reproduced from M. Simon *et al*. *Chem. Sci.*, **2019**, 10, 385 - Published by The Royal Society of Chemistry. [S1]
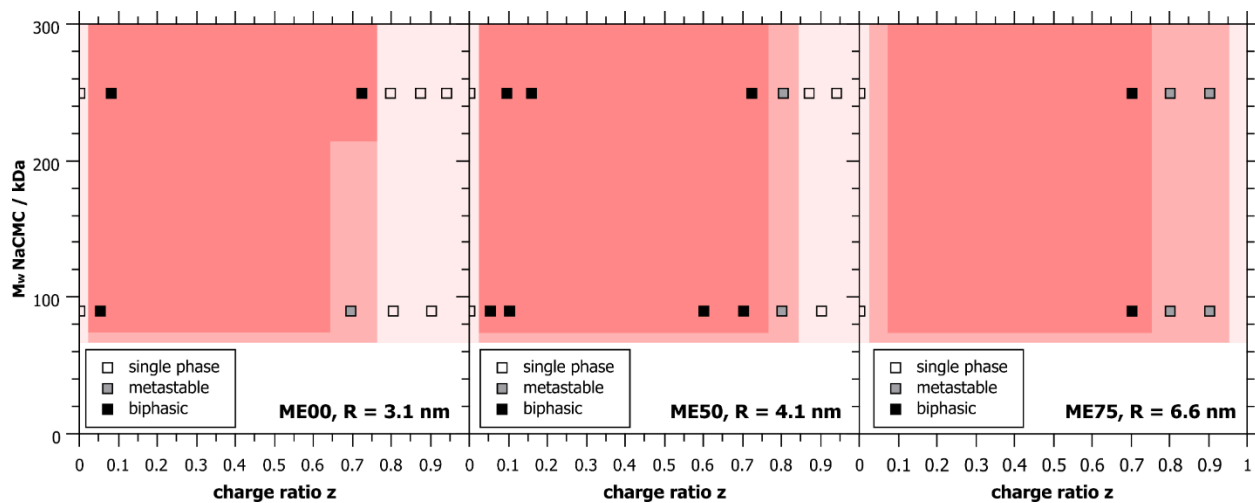
Figure S4: Phase diagrams showing the single phase, metastable and biphasic regions of differently sized microemulsion droplets mixed with NaCMC.

C. Light Scattering Data
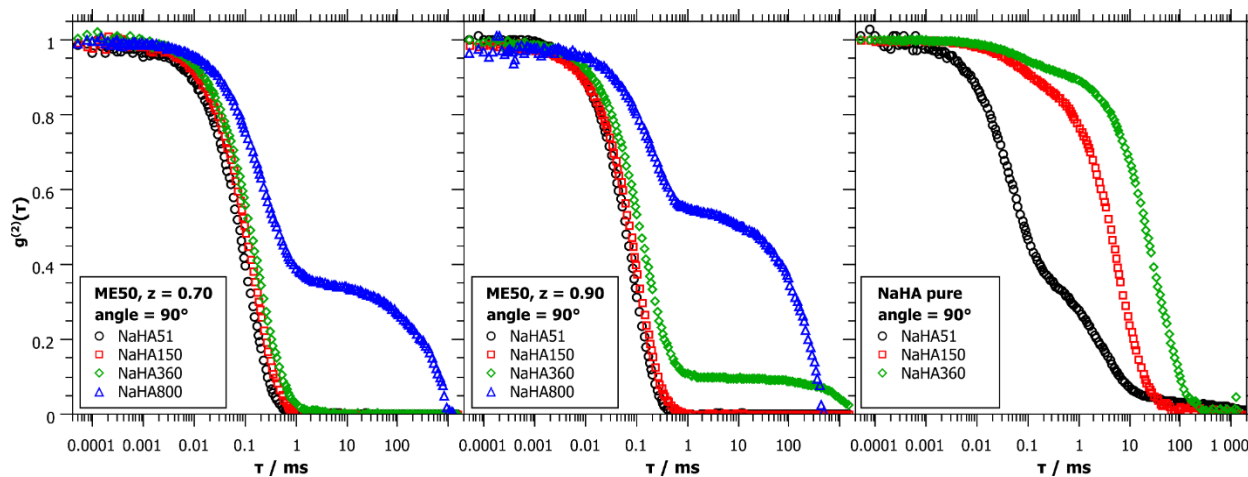
Figure S5: Selected correlation functions of DLS measurements at 90° show the bimodal distribution developing for complexes with higher M_w of NaHA, bimodal distributions are also present for the pure NaHA (pure NaHA, 1 wt%, was measured in PBS buffer). Correlation functions were normalized to 1.
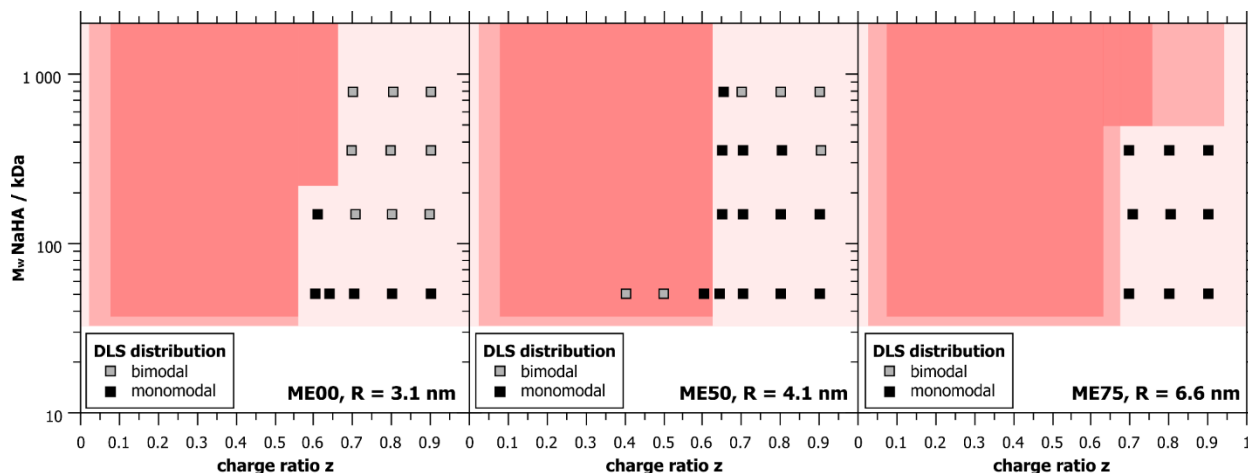
Figure S6: Diagrams showing the distributions of the DLS correlation functions for differently sized microemulsion droplets mixed with NaHA. The distribution was considered bimodal if the stretching exponent α of a monomodal fit became lower than 0.9.

7
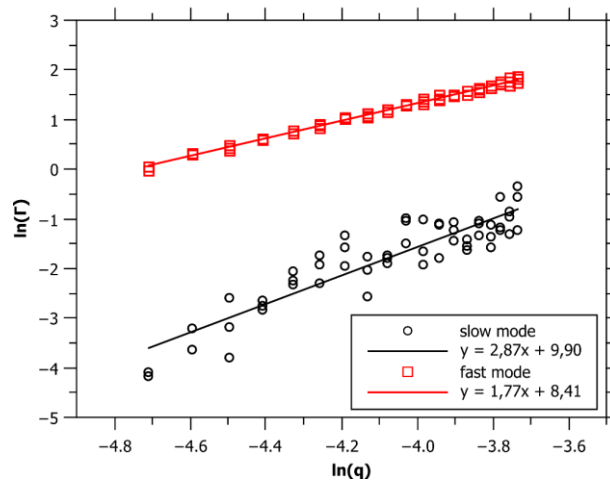
Figure S7: Exemplary plot of ln(Γ) vs. ln(q), showing a dependency close to $\boldsymbol{\Gamma \sim q^2}$ for the fast mode (= free diffusion) and close to $\boldsymbol{\Gamma \sim q^3}$ for the slow mode (= polymer relaxation).
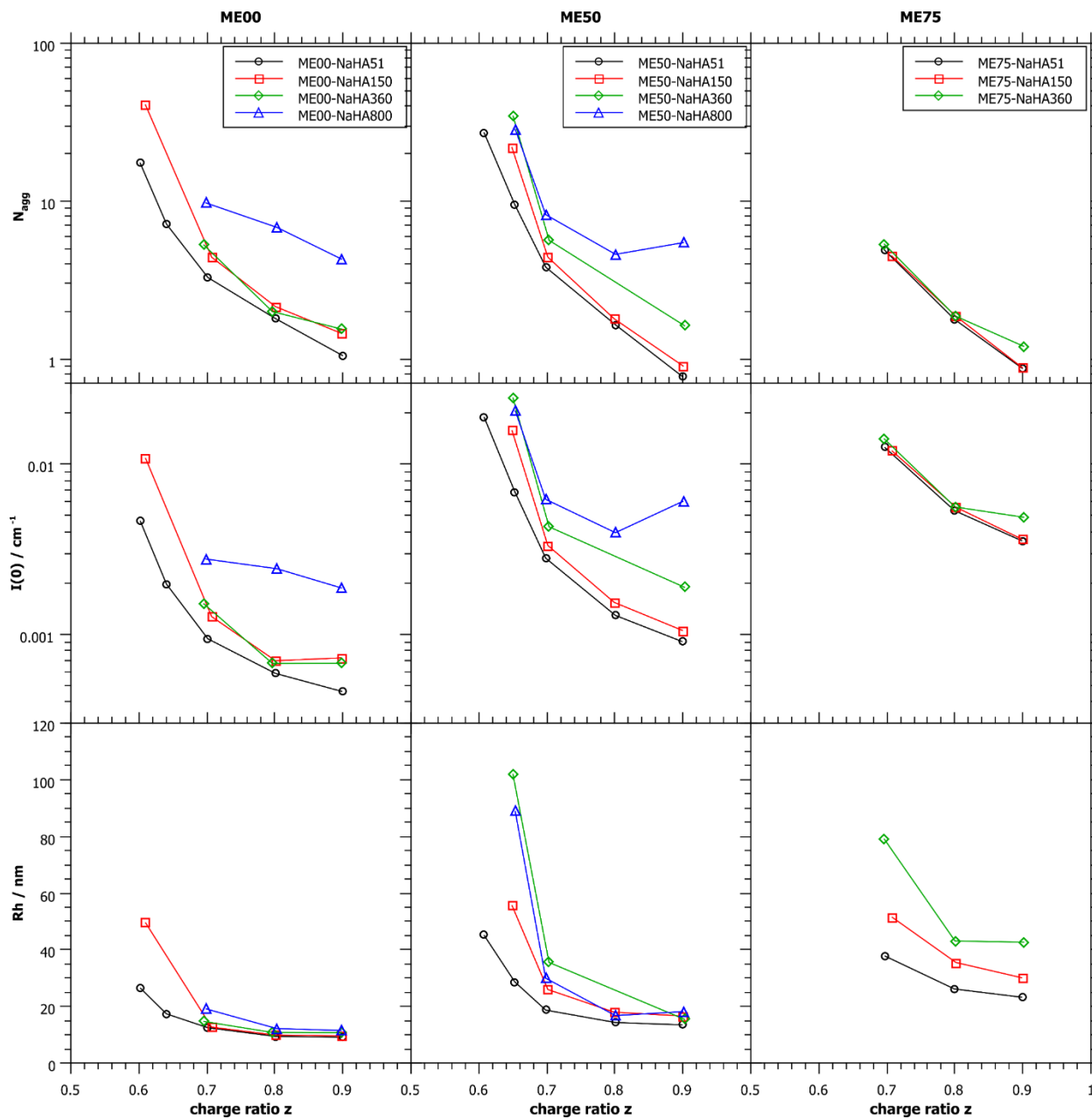
Figure S8: Results from static (top and middle) and dynamic (bottom) light scattering for the differently sized ME droplets.
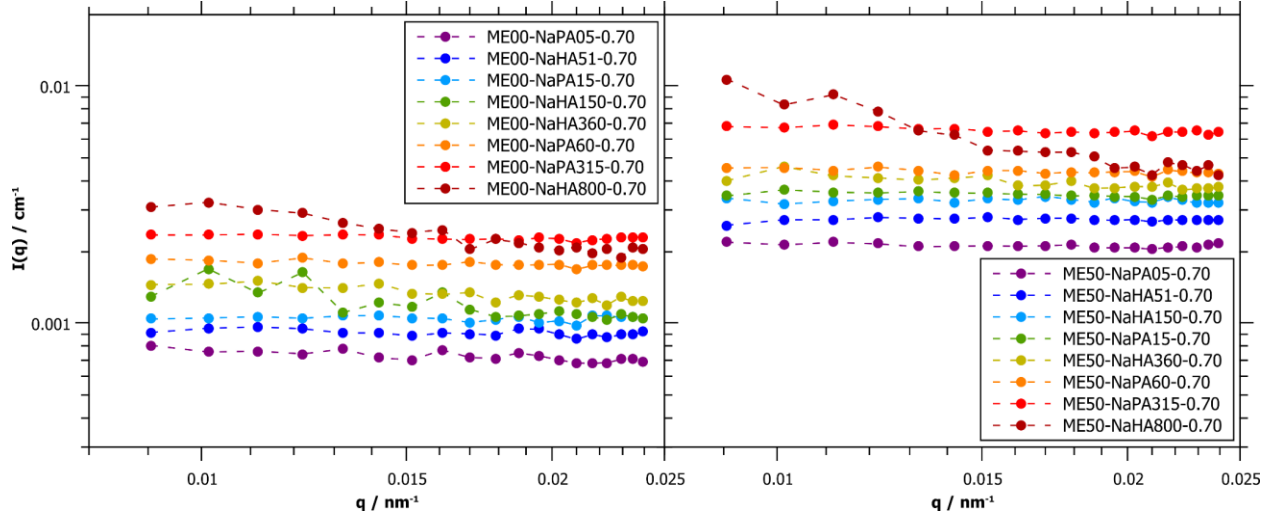
Figure S9: Comparison of static light scattering (SLS) data for small (ME00, R = 3.1 nm, left) and medium-sized (ME50, R = 4.1 nm, right) microemulsion droplets mixed with NaHA and NaPA at z = 0.7 (last number in sample name), close to the phase boundary. For both droplet sizes the same trends in intensity change are seen and one just has higher intensities for the larger droplets. A marked angular dependence can be seen for NaHA800 in both cases, indicating the formation of larger aggregates here.

Table S2: Molecular weights and aggregation numbers for all samples as obtained from SLS.

	z	**ME00** M_w / kg/mol	N_{agg}	**ME50** M_w / kg/mol	N_{agg}	**ME75** M_w / kg/mol	N_{agg}
ME+NaCl	0.00	65.0		175.7		627.6	
NaHA51	0.40_LP			192.9	1.10		
	0.50_LP			201.1	1.14		
	0.60	1129.8	17.38	4755.2	27.07		
	0.65	463.4	7.13	1654.3	9.42		
	0.70	212.4	3.27	668.1	3.80	3060.8	4.88
	0.80	116.8	1.80	288.8	1.64	1117.1	1.78
	0.90	68.3	1.05	135.6	0.77	543.3	0.87
NaHA150	0.60	2643.8	40.66				
	0.65			3835.7	21.83		
	0.70	286.3	4.40	772.2	4.40	2811.9	4.48
	0.80	138.8	2.14			1166.9	1.86
	0.90	94.5	1.45	157.4	0.90	554.7	0.88
NaHA360	0.65			6076.4	34.59		
	0.70	342.0	5.26	990.0	5.63	3347.3	5.33
	0.80	129.7	1.99			1174.5	1.87
	0.90	100.0	1.54	284.2	1.62	750.4	1.20
NaHA800	0.65			4990.5	28.41		
	0.70	632.5	9.73	1438.6	8.19		
	0.80	442.2	6.80	806.2	4.59		
	0.90	278.3	4.28	956.7	5.45		

D. Determination of Diffusion Coefficient of Rods

The determination of diffusion coefficient of rods was done according to Ortega and García de la Torre.[S2]

The diffusion coefficients measured in DLS were interpreted to arise from the diffusion of "effective" rods formed of cylindrically arranged microemulsion droplets. For this treatment, only the fast relaxation rates were used, as the slower ones did not follow the diffusive relaxation law of $\Gamma \sim q^2$ and are assumed to arise from polymer relaxation modes. The translational diffusion coefficient of a rod with a diameter $2R$ of one microemulsion droplet and a certain length L was calculated according to eq. S1:

$$D_t(L) = \frac{1}{3}\frac{kT(\ln p + C_t)}{\pi \eta_0 L} \tag{S1}$$

Where $p = L/2R$ and $C_t = 0.312 + 0.565/p - 0.1/p^2$. $D_t(L)$ was calculated as a function of L and the L-value where $D_t(L) = D_{DLS}$ was determined to be the lengths of the diffusing aggregate.

E. Viscosities
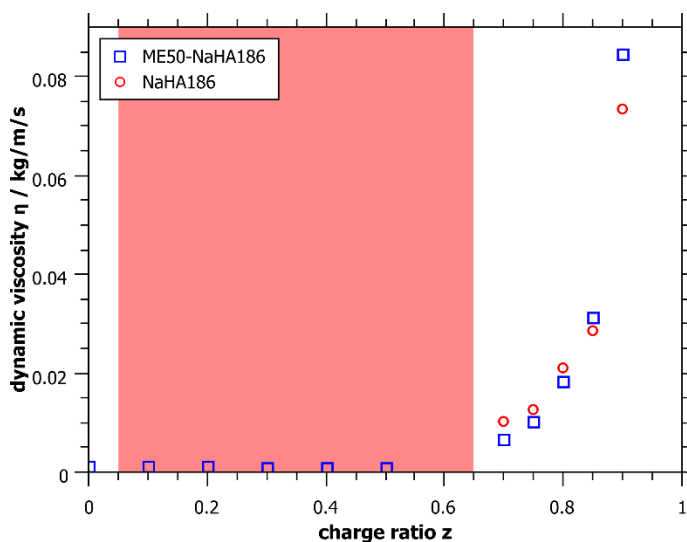
Figure S10: Kinematic viscosities of ME50-NaHA186 samples at different charge ratios z and pure NaHA186 at the respective concentrations. Red background indicates instable samples that were mixed before the measurement and did not phase separate during the measurement time.

F. Description of SANS Models

Form factor: A simple homogeneous sphere model with radius R was assumed for the microemulsion droplets.

$$P(q)_{\text{sphere}} = \left(3 \cdot \frac{\sin(qR) - qR \cdot \cos(qR)}{(qR)^3}\right)^2 \tag{S2}$$

The polydispersity was accounted for by a log-normal size distribution:

$$L_N = \frac{^1 N}{\mu\sigma\sqrt{2\pi}} \cdot \exp\left(-\frac{(\ln\mu - \sigma)^2}{2\sigma^2}\right) \tag{S3}$$

μ and σ are the mean and standard deviation of the log-normally distributed radius R.

$$R = \exp(\mu - \sigma^2) \tag{S4}$$

Homogeneous cylinder model: As a simple approximation of cylindrically arranged microemulsion droplets a homogeneous cylinder model can be applied. Here, the Porod approximation for a long cylinder was used.

Linear arrangement of droplets: The SANS data can also be described with a cylindrical arrangement of microemulsion droplets as was previously done for microemulsion/polyacrylate complexes.[S1] This form factor was previously developed in our group.[S3] The model describes the presence of clusters formed by N aligned particles of radius R and separated by a surface-to-surface distance d. To properly take into account the polydispersity of size and separation distance, the scattering pattern has to be computed by numerically solving the Debye equation. For the calculations, a log-normal distribution of the ME droplet radii, a normal distribution for the border-to-border separation distance and a Poisson distribution for the number of objects forming each cluster, were used. To obtain the scattering curves given in Figure S18, 1000 objects described by distinct values of R, d and N generated by random number generators, were computed and averaged.

New model of curved droplet chains: The Monte Carlo model describes chains of N homogeneous spheres of average radius R, which are separated by an average distance d between the sphere surfaces. Both R and d are polydisperse and randomly picked from normal distributions with standard deviations (σ) corresponding to the polydispersity parameters. R and d as well as their polydispersities were fitted to scattering data of pure microemulsion droplets and then kept constant for all complexed samples of the same microemulsion droplet size. The chains assume the random conformations of semi-flexible polymers of a given persistence length l_{p}. In practice, this is achieved by sampling random conformations while penalizing high angles θ between the vectors between each sphere and its two neighbors with a harmonic constraint potential of adjustable strength V_0:

$$V(\theta) = V_0\theta^2 \tag{S5}$$

The chains are grown stepwise, i.e., sphere by sphere. According the Metropolis algorithm,[S4] the probability of accepting the addition of the next sphere is given by the associated Boltzmann factor $p(\theta) = e^{-V(\theta)/(k_BT)}$. Non-physical conformations with overlapping spheres are excluded. To obtain the scattering curves, at least 5000 conformations are randomly generated in this way. For longer chains (with larger N) comparatively fewer configurations yield the same sampling as comparatively more configurations for shorter chains. The scattering intensities are then computed by calculating the form factor amplitudes of each sphere, subsequent phase-correct summation based on each set of sphere coordinates using the Debye-formula,[S5] and averaging over all conformations.

The stepwise growth of non-overlapping chains employed here is computationally highly efficient but represents the thermodynamic ensemble associated with the angular potential $V(\theta)$ only approximately.[S6] In the main text we therefore do not quantitatively interpret the obtained values of V_0 but instead limit the discussion to the resulting apparent persistence length calculated *a-posteriori* from the ensemble-averaged ratio between contour length L_C and end-to-end distance h, where $\langle h^2 \rangle = 2L_C l_p - 2l_p^2(1 - e^{-L_C/l_p})$.[S7]
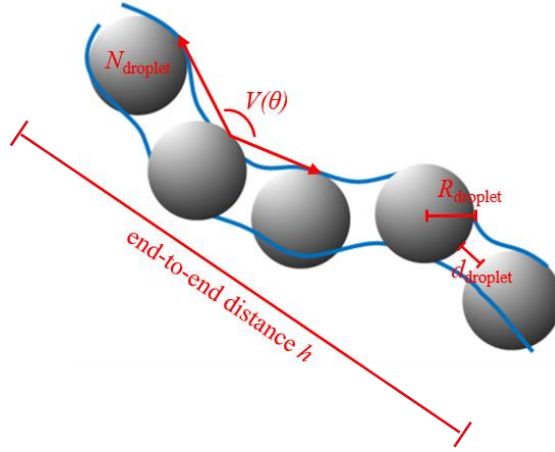
Figure S11: Parameters of the new Monte Carlo model of curved droplet chains.

Scaling of SLS data: The intensity of light scattering data was scaled to match the neutron scattering intensity by accounting for the different contrasts:

$$I(q)_{SLS} \cdot \frac{\lambda^4 \cdot \phi \cdot \Delta SLD^2}{4\pi^2 \cdot n_0^2 \cdot \left(\frac{dn}{dc}\right)^2 \cdot c \cdot \rho} = I(q)_{SANS} \tag{S6}$$

where (dn/dc) is the refractive index increment that was measured by us for the microemulsion and different polyelectrolytes separately. $(dn/dc)_{ME00} = 0.1176 \text{ cm}^3/\text{g}$, $(dn/dc)_{NaPA} = 0.1494 \text{ cm}^3/\text{g}$, $(dn/dc)_{NaHA} = 0.1563 \text{ cm}^3/\text{g}$ and $(dn/dc)_{NaCMC} = 0.1546 \text{ cm}^3/\text{g}$.

G. Additional SANS Data
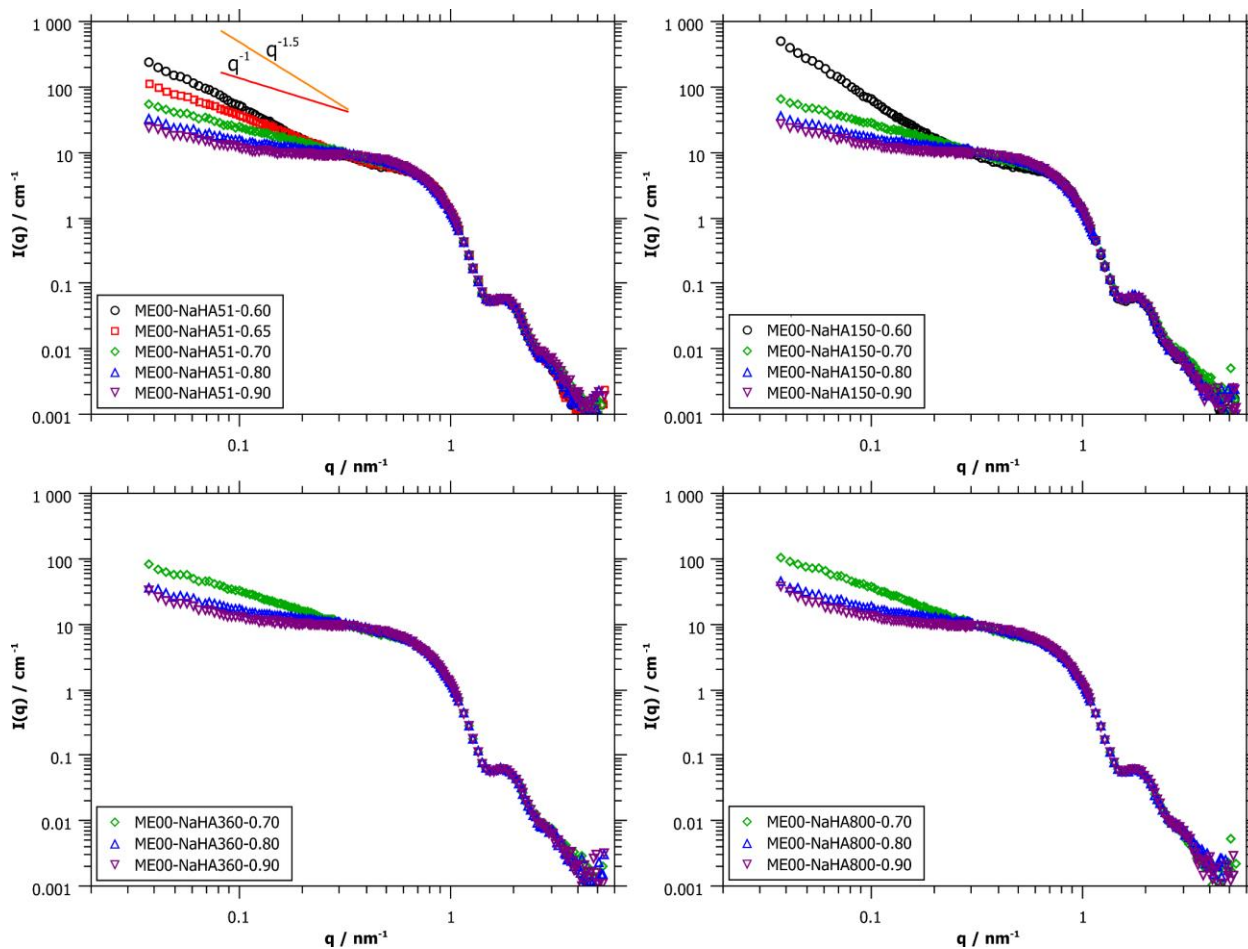
Figure S12 A: full set of all scattering curves for small ME droplets ME00 ($R \sim 3.1$ nm) with different M_w of the NaHA, always as a function of z.
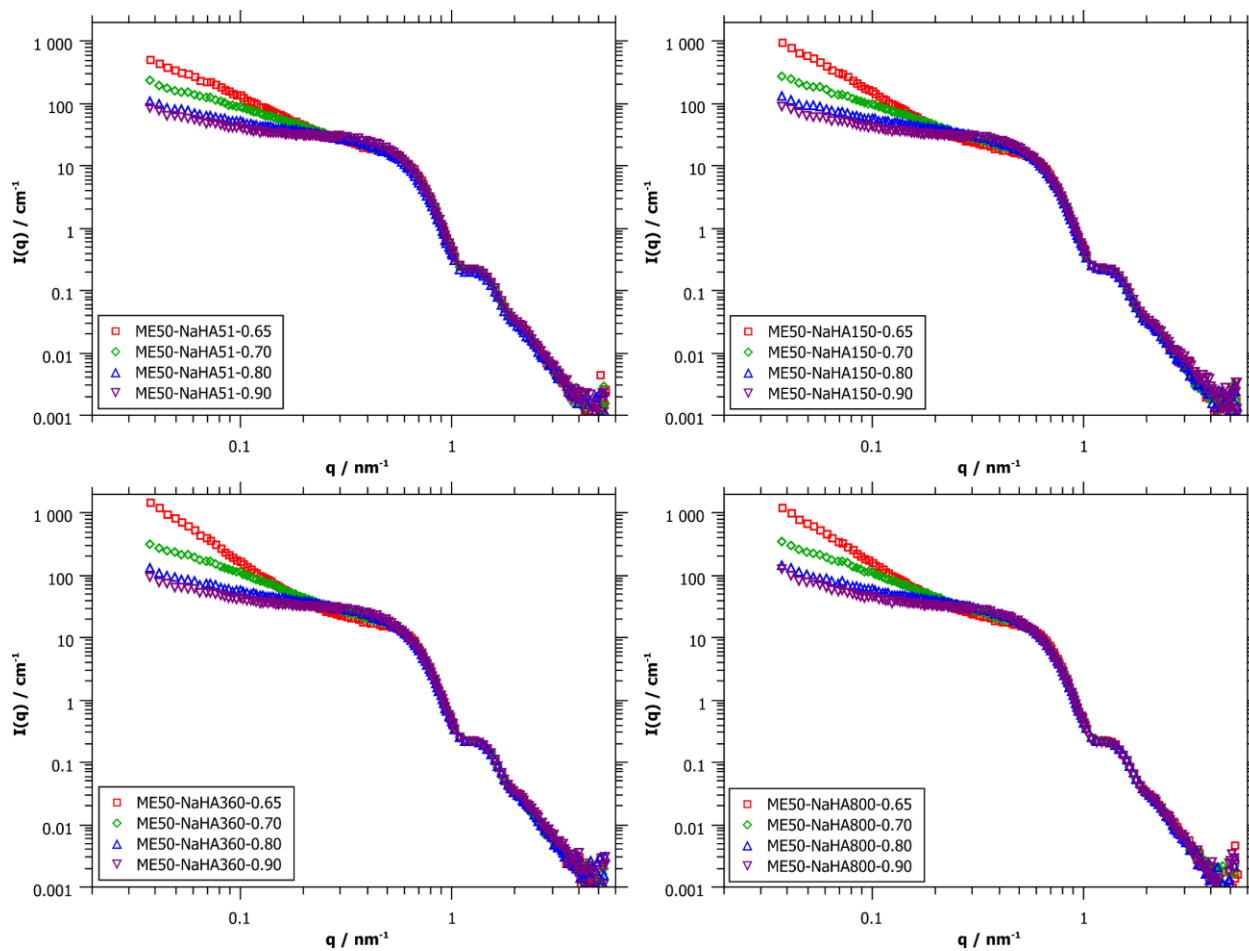
Figure S12 B: full set of all scattering curves for medium sized ME droplets ME50 ($R \sim 4.1$ nm) with different M_w of the NaHA, always as a function of z.
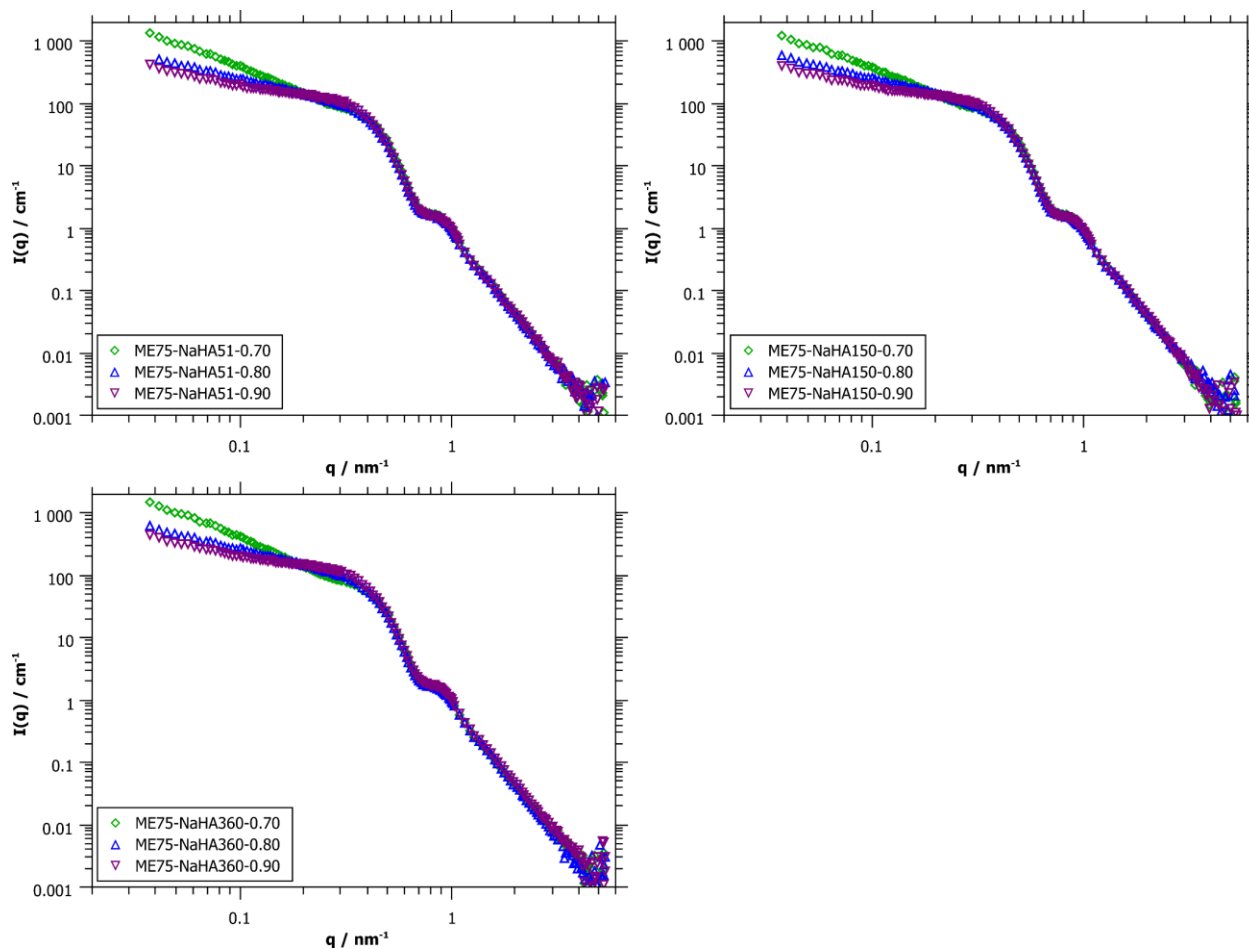
Figure S12 C: full set of all scattering curves for large ME droplets ME75 ($R \sim 6.6$ nm) with different M_w of the NaHA, always as a function of z.
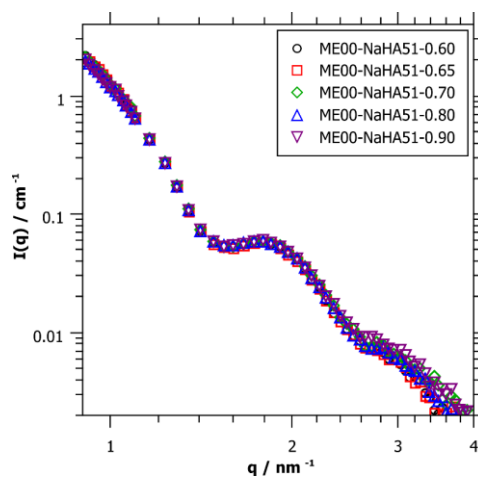
Figure S13: The form factor minimum of the ME droplets in the SANS data does not change upon the addition of PE.
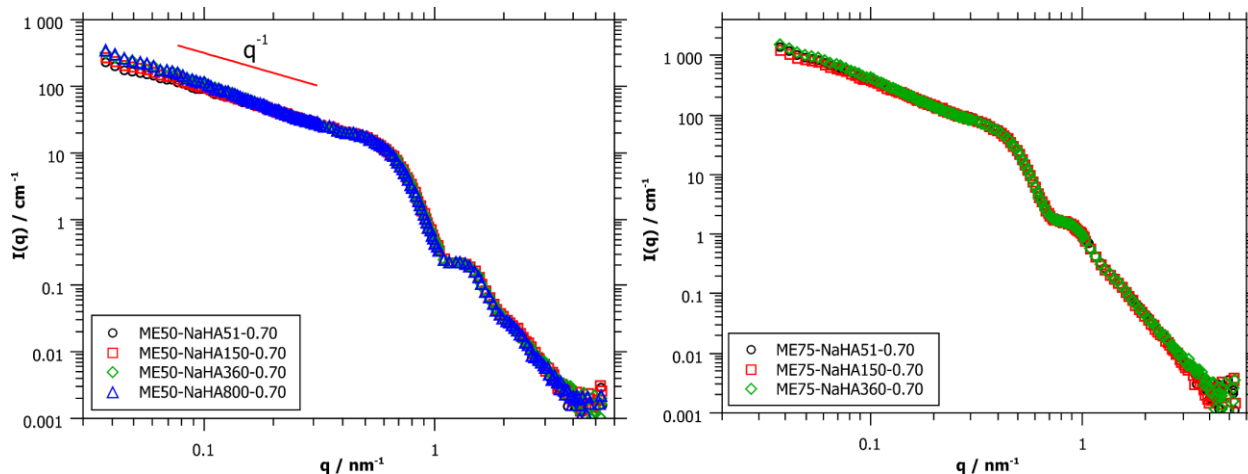
Figure S14: SANS curves on the polyelectrolyte rich side for medium sized microemulsion droplets ($R = 4.1$ nm, left) and large microemulsion droplets ($R = 6.6$ nm, right), both at $z = 0.70$ and different M_w of NaHA. One observes basically identical behavior, irrespective of the M_w of NaHA.
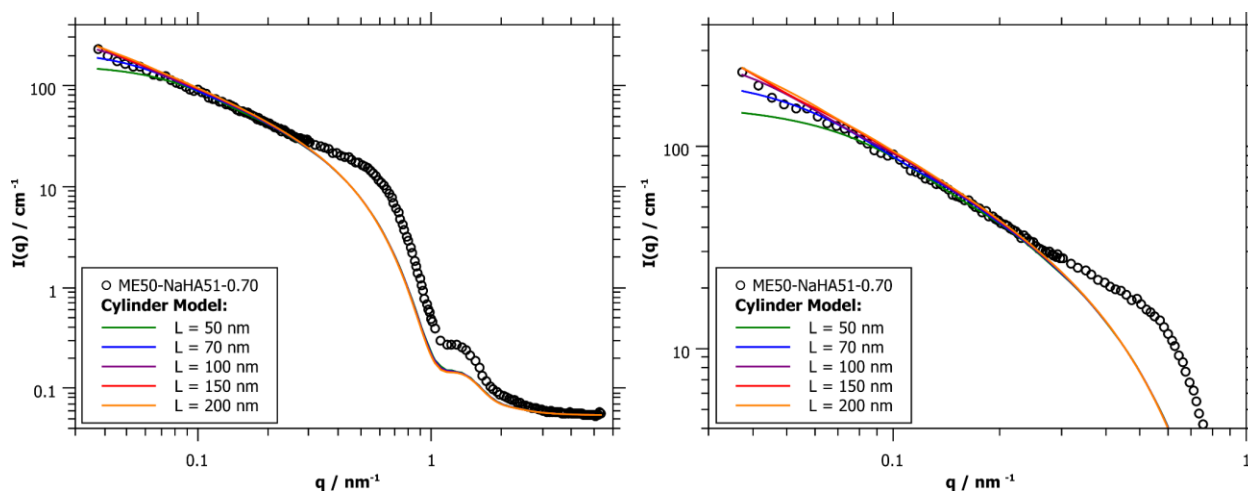
Figure S15: SANS curves of ME50-NaHA51-0.70 sample, solid lines show a cylinder model with different lengths of the cylinder. The radius of the cylinder was chosen to fit the form factor minimum.
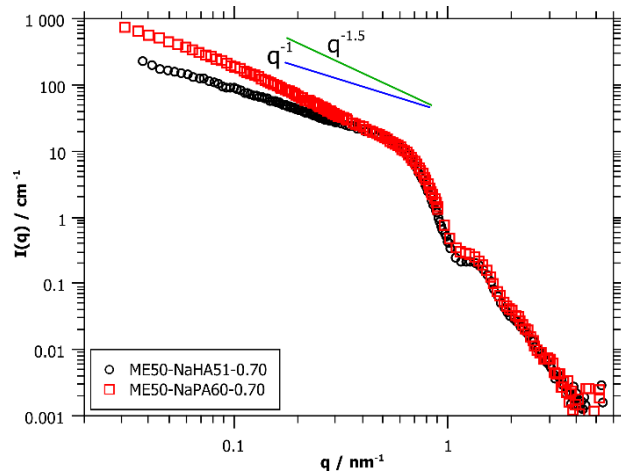
Figure S16: Comparison of SANS data for medium-sized (ME50, R = 4.1 nm) microemulsion droplets mixed with NaHA (M_w = 51 kg/mol) and NaPA (M_w = 60 kg/mol) of comparable length, at z = 0.7, close to the phase boundary. No NaCMC sample is shown here because it was not stable at a mixing ratio of 0.7.
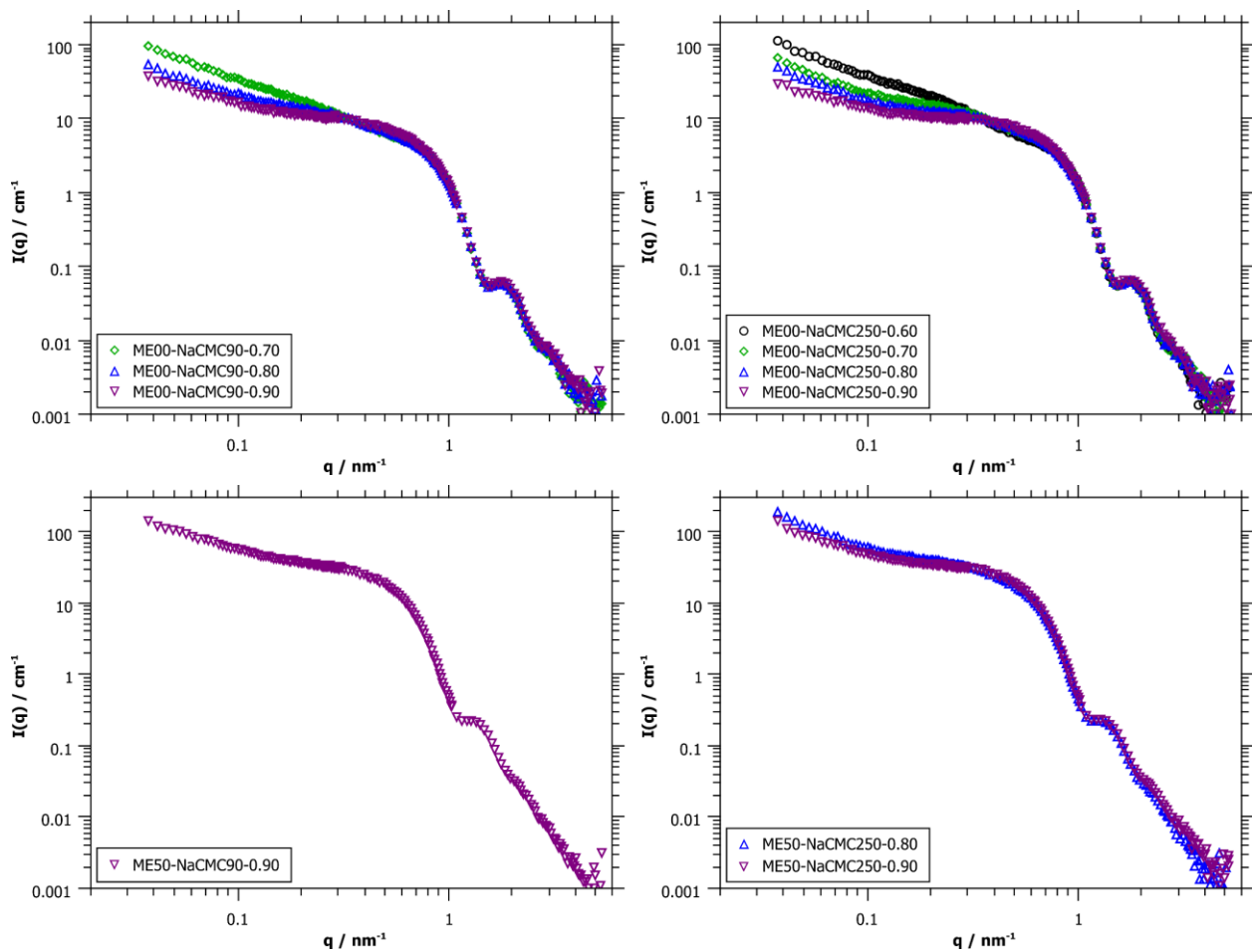
Figure S17: full set of all scattering curves for different M_w of the NaCMC and for differently sized microemulsion droplets and always as a function of z.
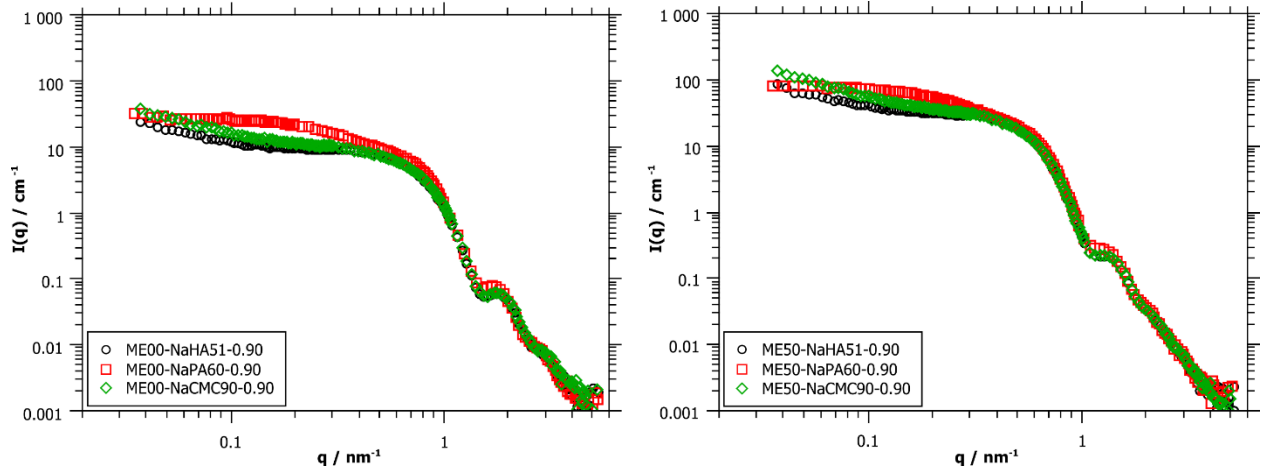
Figure S18: SANS data comparing the different polyelectrolytes at a mixing ratio of $z = 0.9$ for small (left) and medium sized droplets (right).
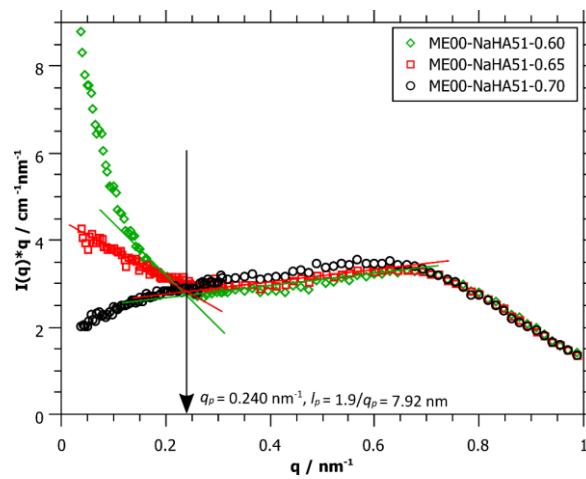
Figure S19 A: Holtzer Plots for SANS data of small microemulsion droplet mixed with short hyaluronate chains at mixing ratios close to the phase boundary.
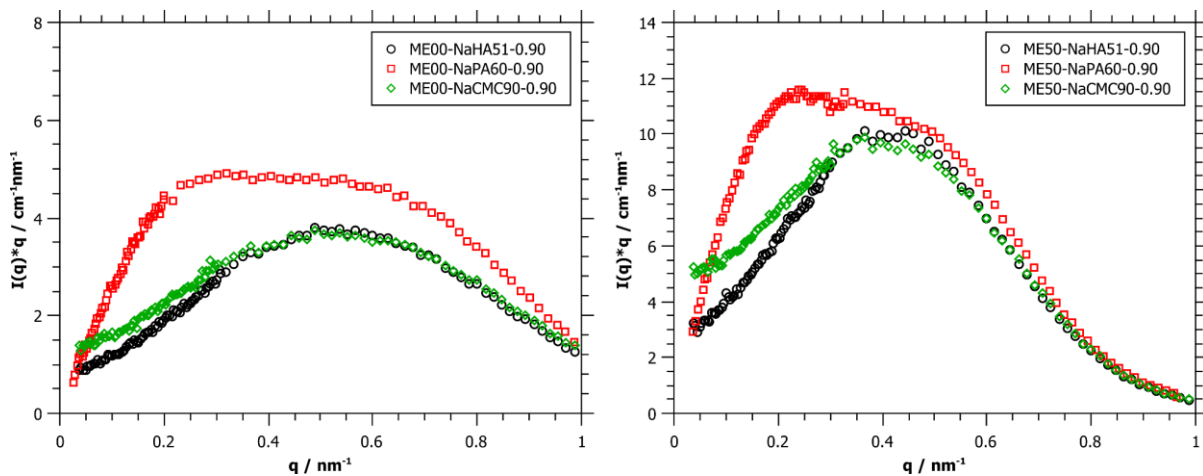
Figure S19 B: Holtzer Plots for SANS data comparing the different polyelectrolytes at a mixing ratio of $z = 0.9$ for small (left) and medium sized droplets (right).
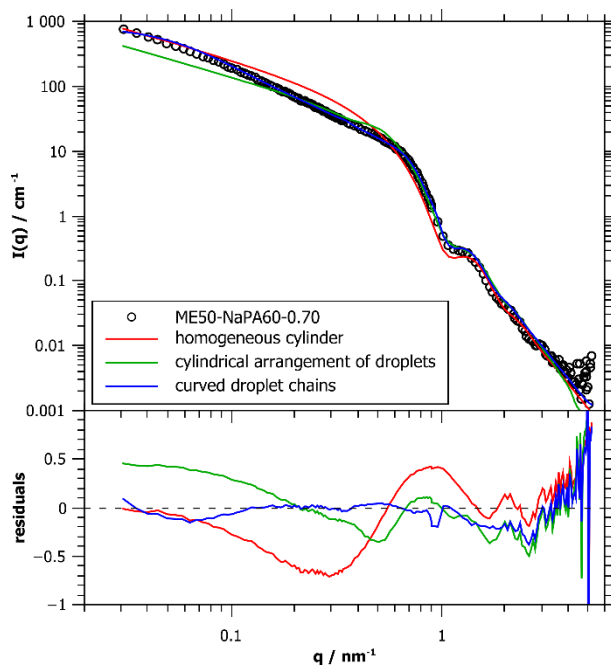
Figure S20: Comparison of different models to describe the SANS data of polyelectrolyte/microemulsion complexes exemplarily for ME50-NaPA60-0.70 sample. It can be seen, that the newly developed Monte Carlo simulation of curved droplet chains describes the scattering data best.
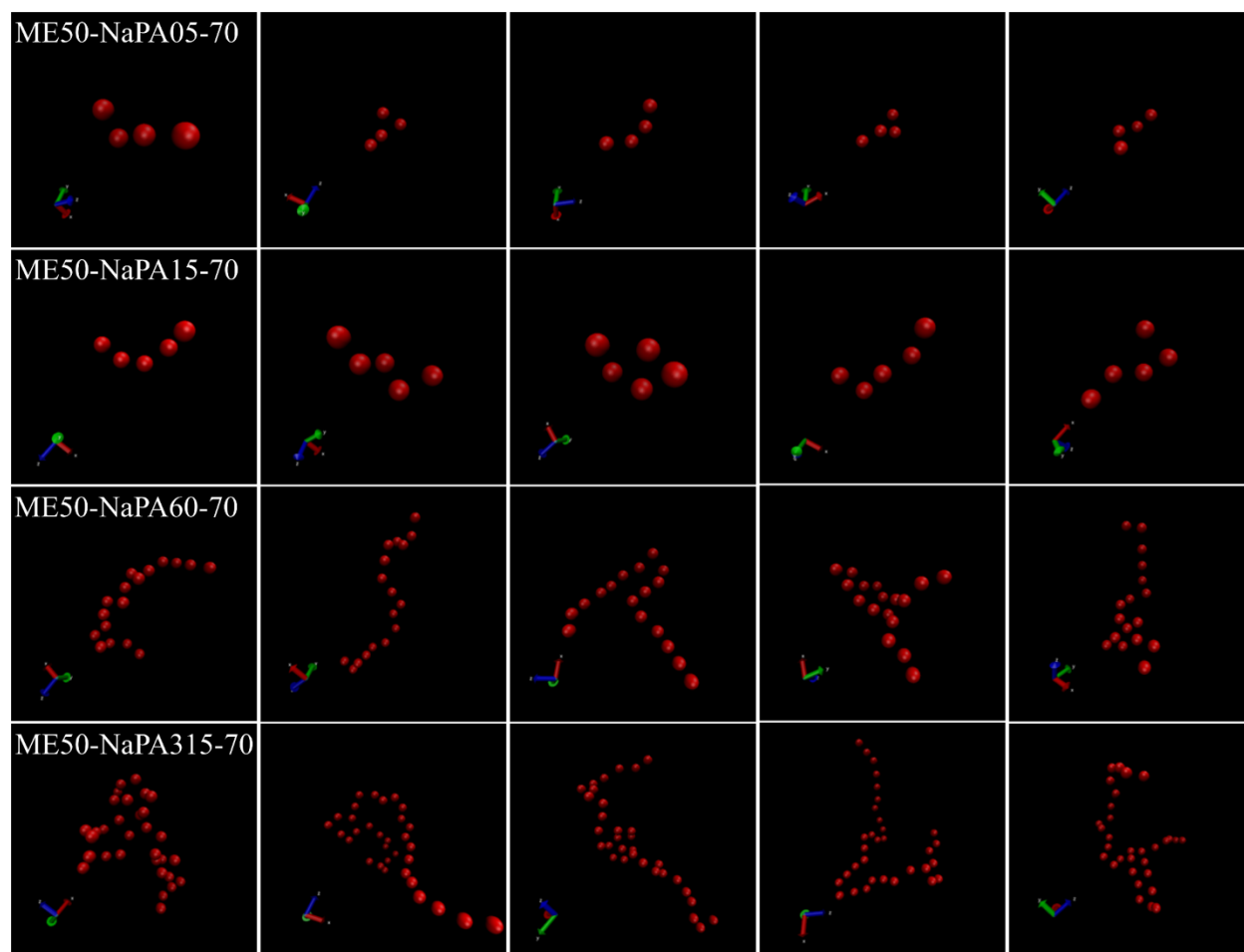
Figure S21 A: Exemplary conformations from the simulations of complexes modelled to describe SANS data of microemulsion droplets aligned in flexible complexes. ME50 (medium sized, $R = 4.1$ nm) was complexed with NaPA of different M_w in a mixing ratio of $z = 0.7$. All parameters except the number of droplets were kept constant in this data set. The persistence length l_p was always ~ 17 nm and one observes well the growth with increasing chain length of the NaPA and the formation of rather bent complexes.
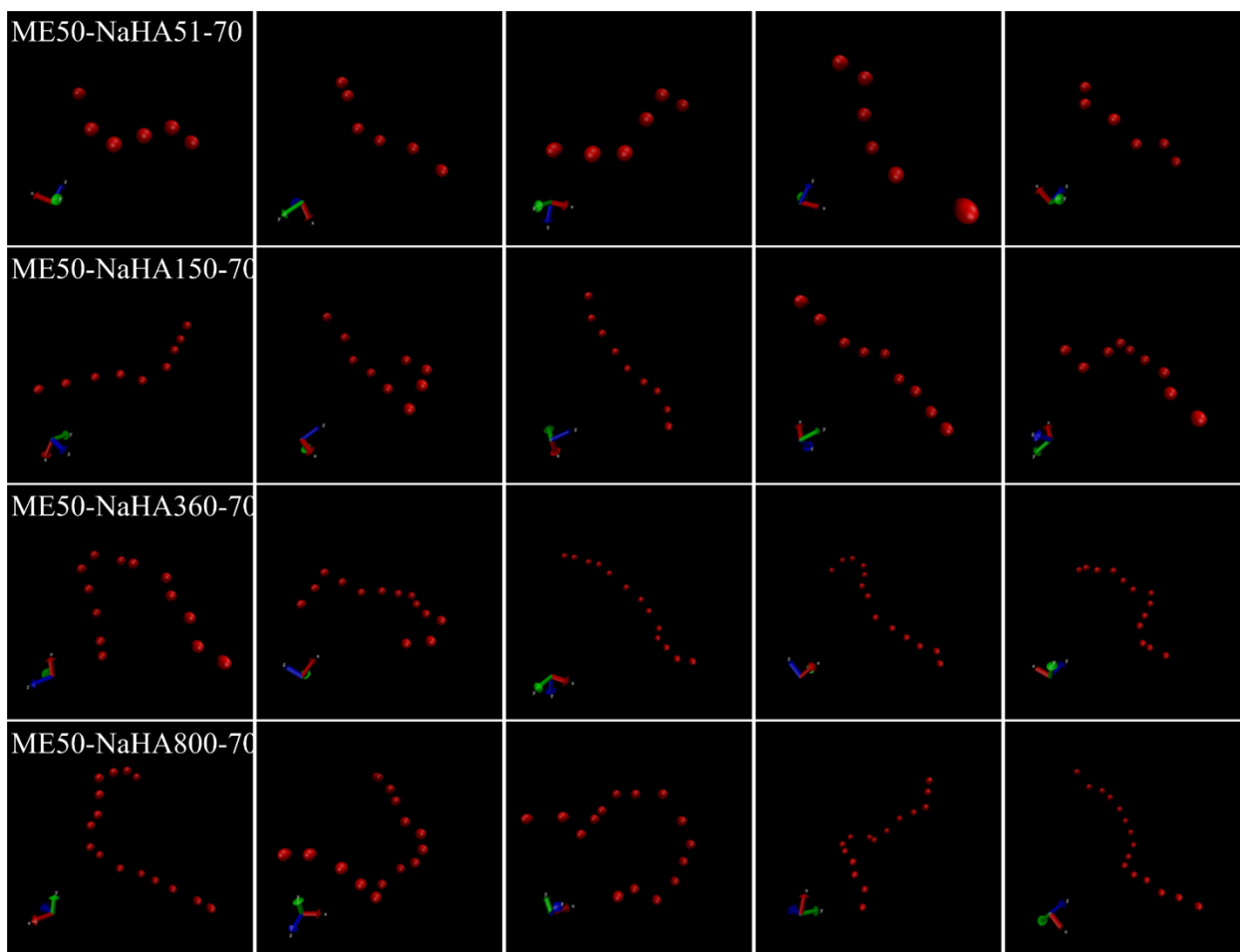
Figure S21 B: Exemplary conformations from the simulations of complexes modelled to describe SANS data of microemulsion droplets aligned in flexible complexes. ME50 (medium sized, $R = 4.1$ nm) was complexed with NaHA of different M_w in a mixing ratio of $z = 0.7$. All parameters except the number of droplets were kept constant in this data set. The persistence length l_p was always ~ 52 nm and one observes well the growth of the complexes and the formation of rather stiff complexes.

H. List of Abbreviations

CMC	carboxymethyl cellulose
NaCMC	sodium salt of carboxymethyl cellulose
NaCMCxx	xx indicates M_w in kDa
cryo-TEM	cryogenic transmission electron microscope
DLS	dynamic light scattering
HA	hyaluronate
NaHA	sodium hyaluronate
NaHAxx	xx indicates M_w in kDa
ME	microemulsion
MExx	xx indicates hexanol content in mM
ME00	small microemulsion droplets, $R \sim 3.1$ nm
ME50	medium sized microemulsion droplets, $R \sim 4.3$ nm
ME75	large microemulsion droplets, $R \sim 6.6$ nm
O/W	oil-in-water
PAA	polyacrylic acid
NaPA	sodium polyacrylate
NaPAxx	xx indicates M_w in kDa
PE	polyelectrolyte
PEMEC	polyelectrolyte/microemulsion complex
SANS	small-angle neutron scattering
SLS	static light scattering
TDMAO	tetradecyldimethylamine oxide
TTAB	tetradecyltrimethylammonium bromide

A	slope
c	concentration
D	diffusion coefficient
d	distance of spheres
DS	degree of substitution
$D_t(L)$	translational diffusion coefficient of a rod
η	dynamic viscosity
Γ	relaxation rate
h	end-to-end distance
$I(q)$	scattered intensity
$I(0)$	forward scattering intensity
k_B	Boltzman constant
L	length of cylinder
λ	wavelength
L_C	contour length
l_p	persistence length
M_w	molecular weight
N	number of spheres
n	refractive index
(dn/dc)	refractive index increment
N_{agg}	aggregation number (droplets per complex)
ϕ	volume fraction
q	magnitude of the scattering vector
R	radius
ρ	density

R_g	radius of gyration
R_h	hydrodynamic radius
SLD	scattering length density
T	temperature
θ	scattering angle
σ	standard deviation
V_0	harmonic constraint potential
z	charge ratio, $z = [-]/([+]+[-])$

References

(S1) Simon, M.; Krause, P.; Chiappisi, C.; Noirez, L.; Gradzielski, G. Structural control of polyelectrolyte/microemulsion droplet complexes (PEMECs) with different polyacrylates. *Chem. Sci.* **2019**, 10, 385-397.

(S2) Ortega, A.; García de la Torre, J. Hydrodynamic properties of rodlike and disklike particles in dilute solution. *J. Chem. Phys*. **2003**, 119, 9914–9919.

(S3) Chiappisi, L.; Prévost, S.; Gradzielski, M. Scattering form factor of N linearly aligned particles forming a cylindrical superstructure. *J. Appl. Cryst*. **2014**, 47, 827-834.

(S4) Metropolis, N.; Rosenbluth, A. W.; Rosenbluth, M. N.; Teller, A. H.; Teller, E. Equation of State Calculations by Fast Computing Machines. *J. Chem. Phys.* **1953**, 21, 1087-1092.

(S5) Warren, B. E. X-ray Diffraction. *Courier Corporation*, **1990**.

(S6) Frenkel, D.; Smit, B. Understanding molecular simulation – from algorithms to applications. *Academic press*, **2002**.

(S7) Hiemenz, P. C.; Lodge, T. P. Polymer chemistry. *CRC press*, **2007**.